Assessment of the seismic behavior of reinforced concrete elements affected by corrosion: An objective comparison between quasi-static and dynamic tests

Chaymaa Le Jouad, Benjamin Richard, Philippe Mongabure, Sophie Capdevieille, Frederic Ragueneau

Assessment of the seismic behavior of reinforced concrete elements affected by corrosion: an objective comparison between quasi-static and dynamic tests

C. Lejouad [1], B. Richard [2*], P. Mongabure [1], S. Capdevielle [3], F. Ragueneau [4]

[1] Atomic Energy and Alternative Energies Commission, CEA, D36, F-91191 Gif-sur-Yvette, France
[2] Institut de Radioprotection et de Sûreté Nucléaire (IRSN), PSN-EXP, SES, LMAPS, 31 avenue de la Division Leclerc, F-92260, Fontenay- aux-Roses, France
[3] Université Grenoble Alpes, CNRS, Grenoble INP, 3SR, 621 Avenue Centrale, F-38400 Saint-Martin-d'Hères, France
[4] LMT, ENS Paris-Saclay, CNRS, Université Paris-Saclay, 61 Avenue du Président Wilson, F-94235 Cachan, France

E-mail addresses: chaymaa.lejouad@gmail.com (C. Lejouad), benjamin.richard@irsn.fr (B. Richard), philippe.mongabure@cea.fr (P. Mongabure), sophie.capdevielle@univ-grenoble-alpes.fr (S. Capdevielle), frederic.ragueneau@ens-paris-saclay.fr (F. Ragueneau).

* Corresponding author

Abstract

Corrosion of steel reinforcement is one of the most widespread pathologies that leads to a loss of structural performance of reinforced concrete (RC) members. Thus, understanding the mechanical consequences of this pathology is of great importance. In the past decades, many studies have been performed to assess the influence of the reinforcement corrosion on the quasi-static behavior of RC structures. However, few investigations have been carried out to characterize the corroded structural dynamic behavior under extreme loading. In this study, the case of the earthquake loading is investigated. The objective is to provide the scientific community with reference experimental data to assess the influence of corrosion on the dynamic properties of structural members. These experimental data are very valuable when calibrating numerical models aiming to determine some significant engineering demand parameters (EDP) such as the bearing capacity, the ductility and the dissipation ability. Furthermore, the relevance of the use of quasi-static tests in predicting the seismic behavior of corroded RC elements is assessed. To reach this goal, an experimental campaign is conducted on large-scale RC beams. The corroded and non-corroded beams are subjected to a four-point bending test and to dynamic loads on the AZALEE shaking table (keeping the same loadings and boundary conditions). In this paper, a detailed description of the experimental campaign is presented. Then, the results are exposed, showing the influence of the corrosion rate on the bearing capacity, hysteretic response, ductility offer, eigenfrequencies and damping ratios.

Keywords: Steel corrosion, shaking table, reinforced concrete, aging

1. Introduction

Reinforced concrete (RC) has been the most widely used construction material for many decades. It is commonly used for buildings as well as nuclear facilities. This is mainly due to its low cost, good mechanical properties, and satisfactory durability properties. However, the service-life of RC structures may be reduced along with time, due to the emergence of pathologies. Among them, the steel reinforcement corrosion is one of the major pathologies, which makes the structural performance decrease. This phenomenon can lead in its early stages to a loss of durability at the material scale, a loss of service ability and lately, a loss of structural safety.

In the civil engineering field, the steel reinforcement corrosion is a concern, especially for RC structures located in marine environment. For this reason, the infrastructure operators are required to carry out maintenance operations throughout the structure lifetime. Based on structural auscultation, these operations seek to restore the initial structure bearing capacity without considering the dynamic response, less well known in the case of corrosion pathology. Hence, the study of the effect of corrosion

on the dynamic behavior of RC structures is of crucial importance to perform efficient maintenance operations. The latter are determined, in practice, by the means of numerical models which need to be calibrated based on experimental data. In this context, this study aims at expanding the available datasets regarding the static and dynamic response of corroded RC members.

Corrosion in reinforced concrete is caused by the introduction of some aggressive agents from the external environment, reaching the steel bar surface through the concrete pores. In this context, two types of steel corrosion can be distinguished: a first type resulting from a carbon dioxide dissolution and a second due to chloride penetration [1]. In case of corrosion induced by carbonation, also called uniform or generalized corrosion, one can observe a homogeneous distribution of the cross-section loss along the steel bar. In case of corrosion induced by chlorides, also called pitting or localized corrosion, the morphology of corroded bars shows a localized loss of cross section. As a result, this second type of corrosion seems to be the most harmful for reinforced concrete structures [2]. That is why the present study focuses on the chloride-induced corrosion.

Corrosion in RC structures is a process which takes a long period of time: a study carried out on a RC specimen subjected to natural corrosion shows that after 16 months of exposure the degradation of the specimen remains insignificant [3]. In the research field, using natural corrosion process to get corroded specimens is time demanding. That is why the research community has come up with some technics to accelerate corrosion. One can cite the galvanostatic method (whether by imposed current [4] or imposed voltage [5]), the artificial environment [6] [7], and additives in concrete mixture [8] [9]. The differences between each accelerated corrosion technique and the natural corrosion process have been widely discussed in the literature.

The use of additives in concrete mixture is highly criticized. Indeed, by using this accelerated technique, the concentration of chlorides is relatively constant on the bar surface and the obtained concrete is more porous [10]. This observation is not in accordance with the fact that the natural corrosion process occurs by the local introduction of chlorides through the pores of the concrete cover. The artificial environment corrosion technique is the closest to the natural corrosion regarding the mechanical consequences and the electrochemical process. It can be assimilated to the natural corrosion phenomenon occurring in tidal area in a bridge pier for instance. However, it is still a time consuming process with no access to the final corrosion ratio unless destructive tests are performed [11]. The main advantages of the galvanostatic method are a great time saving and a direct access to an estimation of the induced corrosion ratio without any further investigations. That is why this technique has been chosen for the present work. Many studies have shown that the choice of the current density value has a direct consequence on the more or less similitude with natural corrosion regarding crack patterns for example. Most of the existing studies suggest not to exceed 100 $\mu A.cm^{-2}$ to have similar structural effects as natural corrosion [12] [13], even if the corrosion products are slightly different.

In terms of the mechanical response of corroded RC structures, several experimental campaigns have been conducted. Experimental campaigns dealing with quasi-static loadings have been widely achieved in the literature. These campaigns considered different types and dimensions of specimens varying from small scale beams [14] to large scale columns [15]. The corroded specimens using the suitable accelerated corrosion technique are subjected to monotonous static loadings in the majority of cases [16] [11] [17] and less frequently to cyclic static loadings [18] [19] [15]. In the study carried out by [11] for example, 3 m long corroded beams were subjected to a 3-point bending load. A loss of the structure load-bearing capacity, elongation at failure, and stiffness have been observed. The authors of [20] have tested 13 circular corroded RC columns under cyclic loading. A decrease of the loading capacity, the evolution of ductility and the stiffness, and the energy dissipation with an increasing corrosion ratio have been observed. The study of [18] came to confirm these observations. The experimental results analysis demonstrated a reduced hysteretic response, a decrease of ductility and a drop in the energy dissipation capability for the highly corroded columns, compared to the non-corroded ones.

Dynamic loadings, on the other hand, have been used in a very limited number of studies [21]. Therefore, the dynamic properties (such as the equivalent damping ratio) of RC elements are deduced from the quasi-static cyclic response. Among the existing studies, an experimental campaign was carried out by [22] on corroded RC frames using accelerated corrosion by imposed current technique in order to assess the influence of corrosion on the modal properties of RC structures. Using hammer shock tests, the determination of both the eigenfrequency and the modal damping ratio was possible. At low level of loading, an increase in the fundamental frequency and the damping ratio is observed for an increasing corrosion degree. However, at a critical corrosion degree, these quantities of interest tend to decrease. Different results were addressed in another study [23]. In [21], shaking table tests were performed on corroded bridge piers. A decrease in both shear and flexural capacity as well as an increase in the natural period and the damping ratio have been observed as the corrosion severity gets worst.

Since dynamic tests are few and very expensive, the experimental campaigns using cyclic loadings are a significant means to predict the dynamic response of structures. However, some aspects are not taken into account in such experiments, like the inertial effect or viscous phenomena. The present paper intends to fill this gap. An experimental campaign is carried out on 18 large-scale corroded RC beams, in addition to 2 reference beams. The specimens are corroded using an induced current corrosion technique at three different corrosion rates and three reinforcement corrosion configurations. The corroded beams are then subjected to cyclic four-point bending tests as well as dynamic loadings on the shaking table considering the same experimental setup. This study aims to:

(1) extend the available experimental database concerning the static and dynamic behavior of corroded RC members;
(2) assess the effect of corrosion on the dynamic properties (eigenfrequency and damping ratio) of RC members;
(3) compare the experimental results (bearing capacity, ductility, hysteretic response…) resulting from quasi-static cyclic tests with the ones resulting from dynamic tests, considering the same experimental set-up;
(4) give a new and innovative insight on the reliability of commonly used damage indicators, such as the element's natural frequency drop-off and modal damping ratio, in case of corroded RC members.

This paper will first give a detailed overview of the carried out experimental campaign. Then, the experimental results in terms of static and modal properties, obtained from quasi-static as well as dynamic testing, are underlined. Finally, the concordance between the results obtained from dynamic and quasi-static testing is evaluated.

2. Experimental campaign

2.1. Scope

The experimental campaign DYSBAC, a French acronym for "Dynamic behavior of corroded RC structures", is performed by means of the AZALEE shaking table and the strong floor, which are parts of the TAMARIS experimental facility operated by the French Alternative Energies and Atomic Energy Commission (CEA) located in Saclay, France. The main objective of this experimental campaign is to study the influence of corrosion on the dynamic behavior. In particular, the natural frequencies and damping ratios are investigated. The quasi-static behavior is also studied in order to determine whether the prediction of the dynamic response is possible through a quasi-static test.

2.2. Specimens

In order to be representative of real RC structures and overcome any scale effect, the choice of large-scale RC beams has been made. The geometry of the DYSBAC specimens has been designed considering the constraints related to the test facilities. The beam length was set at 4.5 m in order to conform to the strong floor dimensions. The maximal stroke of the available actuator ($\pm$ 500 mm) and

the will to reach the beam failure were decisive parameters in the choice of the cross-section dimensions and the considered reinforcement. The beam design matches with the technical requirement of the AZALEE shaking table. Especially, its operating frequency range is in between 0.5 Hz and 30 Hz in order to ensure that the target seismic inputs can be accurately realized. With these constraints, each beam is 4.5 m long with a cross-section of $200 \times 400\ mm^2$ as shown in Figure 1. a.

The reinforcement pattern, as presented in Figure 1. b, is designed according to the European standards Eurocodes 2 and 8 [24] [25]. The steel reinforcement consists of ribbed B500A steel bars according to the French steel classification NF A 35-080-1 [26], with a minimum yield strength equal to 500 MPa and an ultimate strain (A_{gt}) higher or equal to 2.5 %. 4 bars of 12 mm diameter constitute the longitudinal reinforcement, whereas the transversal reinforcement is formed of 8 mm diameter stirrups with a spacing of 100 mm. The concrete cover is 30 mm.

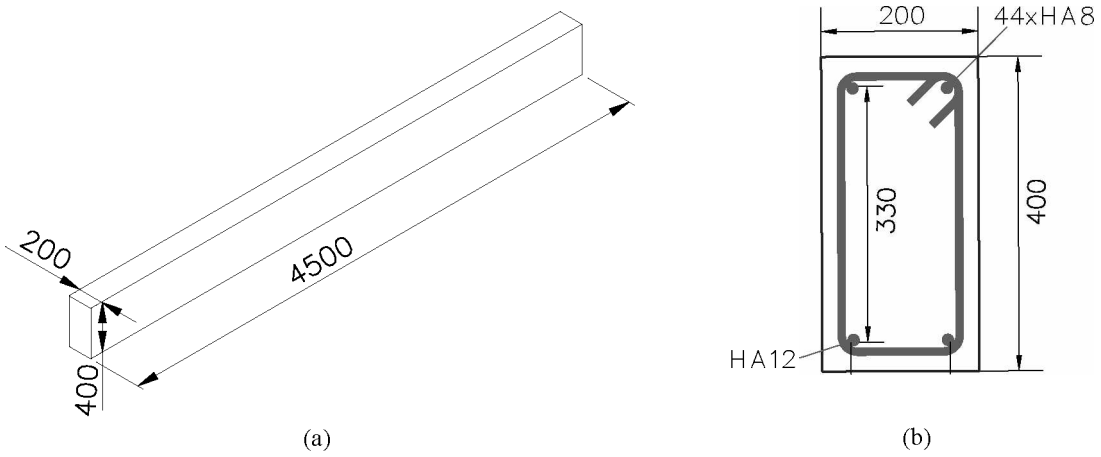

Figure 1: Specimen's design: (a) Geometry, (b) Reinforcement details. - dimensions in millimeters -

The 20 specimens are cast with a C25/30 concrete class according to the Eurocodes 2 [24]. The considered concrete is formulated with a high water cement ratio of around 0.6. This leads to a porous and low strength concrete, representative of concrete in aged RC structures. The mean concrete properties, measured on 12 cylinders (ϕ 16 cm, height 32 cm), are presented in Table 1.

Table 1: Concrete characteristics measured on cylinders.

	Compressive strength (MPa)	Tensile strength (MPa)	Young modulus (MPa)
Mean	35.6	2.6	23 200
Standard deviation	0.6	0.2	543.1

2.3. Sample corrosion

Based on the overview of the accelerated corrosion methods provided in the introduction section, the induced corrosion by imposed current technique was used [15]. By using this method, the exposure time was highly reduced. Moreover, the targeted corrosion rates are easier to reach by choosing the suitable parameters (the exposure time and the current density), which might not have been the case if other accelerated corrosion techniques had been used. The corrosion phenomenon is fully driven by the electron flow or, in other words, by the electrical current intensity [27]. For this reason, the imposed current method was preferred to the induced corrosion by imposed voltage method.

The imposed current technique consists in applying an electrical current from a Direct Current (DC) power supply between the cathode, which is a stainless steel grid, and the anode, which is the reinforcement inside the RC specimen [13]. The whole specimen is immersed in an electrolytic solution containing chlorides in order to ensure electrical conduction and to be representative of corrosion by chlorides. Figure 2. a is a simplified representation of the accelerated corrosion by imposed current setup. Figure 2. b is a top view of campaign beams subjected to accelerated corrosion technique.

(a) (b)

Figure 2: Accelerated corrosion technique: (a) Simplified setup, (b) Corrosion of the specimens.

One of the study objectives is to separately assess the effect of corrosion of the different reinforcement parts (longitudinal and transversal reinforcements) on the mechanical response of the specimens. For this reason, three beam configurations are considered:

- C_1 for the longitudinal reinforcement corrosion;
- C_2 for the stirrups corrosion;
- C_3 for the full reinforcement corrosion.

In order to reach the corrosion targets for the three configurations, different parts of reinforcement were electrically insulated and different cathode settings were adopted, depending on the configuration. The insulation consists of putting an electrically insulating paint and some heat-shrink cable sleeve on each contact zone to be insulated. Electrical connection is achieved by drilling the reinforcing bar and welding an electrical wire. To make sure of the good behavior of the insulation and the electrical connection, a preliminary experiment was performed on a bare reinforcing cage with insulation.

For the C_1 beam configuration:

- an insulation is put on the stirrups to keep only the longitudinal bars crossed by the electrical current;
- each longitudinal bar is considered as an anode with an independent cathode made of stainless steel (Figure 3. a);
- a four channels DC power supply is used.

For the C_2 beam configuration:

- the insulation is put on the longitudinal bars at the connecting points with the stirrups. In this way, only stirrups are crossed by the electrical current;
- the full beam is wrapped with the stainless steel grid (Figure 3. b);
- one DC power supply is used.

For the C_3 beam configuration:

- no insulation is put;
- the full beam is wrapped with the stainless steel grid (Figure 3. b);

- one DC power supply is used.

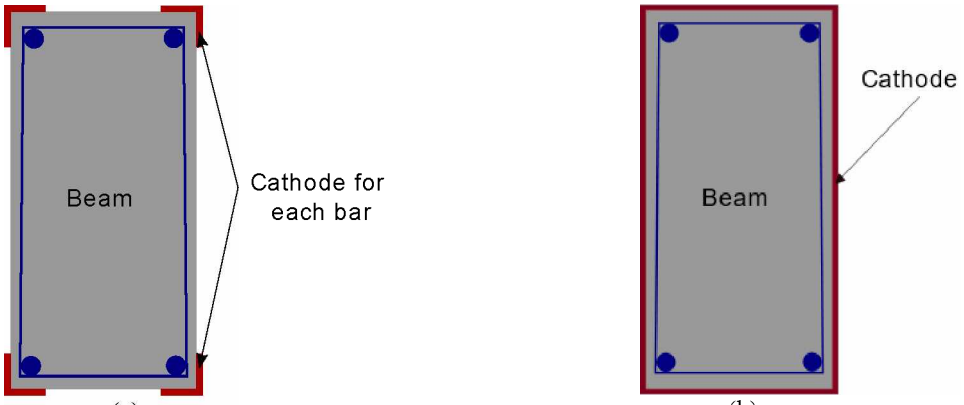

Figure 3: Cathode position : (a) C_1 configuration (b) C_2 and C_3 configurations.

As recommended in [28], the current density was limited to 100 $\mu A.cm^{-2}$ in order to obtain representative rust close to natural oxidation products. It is important to note that despite the fact that the chemical nature of rust product is not strictly equivalent to the one observed in case of natural corrosion, the mechanical consequences are the same [29]. Three corrosion rates, expressed in terms of mass loss are targeted:

- 5 % , because many studies demonstrated a degradation of the bond between steel and concrete for a corrosion rate between 1.5 % [30] and 5% [31] [32];
- 10 % , rate from which civil engineering maintenance operations start [33] ;
- 15 % , demonstrated in some studies to be the threshold from which a change of the steel failure mode is observed [34] [35].

All the beams are immersed in a 3.5 % NaCl solution (Figure 2. b). The exposure duration is estimated for each type of beam and each corrosion rate using Faraday's law (Equation 1) with $\alpha = 1.3$.

$$\Delta t = \frac{\alpha .\Delta w .z.F}{M.I} \qquad (1)$$

where Δw is the mass of steel consumed due to corrosion (kg.m^{-2}), I is the current density (A.m^{-2}), Δt is the exposure time (s), F is the Faraday constant 96 500 (C.mol^{-1}), z is the ionic charge (2 for F_e), M is the atomic weight of steel (g.mol^{-1}), α is a coefficient usually taken between 1 and 2 to take into account the duration of chloride ingress into concrete before reaching the rebar. Table 2 sums up the estimated exposure time for each corrosion degree and each beam configuration.

Table 2: Exposure duration for different beam configurations.

Configuration C_1		Configuration C_2		Configuration C_3	
For each bar HA12		44 stirrups HA8		4 bars HA12 and 44 stirrups HA8	
Corrosion rate (%)	Exposure duration (days)	Corrosion rate (%)	Exposure duration (days)	Corrosion rate (%)	Exposure duration (days)
5	47	5	31	5	36
10	94	10	62	10	72
15	141	15	94	15	109

For the sake of clarity, each beam has been labeled with respect to its corrosion configuration (C_1, C_2 or C_3) followed by the targeted corrosion rate (5 %, 10 % or 15 %). To be more specific, the label Cn_R refers to the configuration n and to the corrosion rate R. For example, the label C1_15 corresponds to a longitudinal corrosion beam corroded at 15 %.

2.4. Setup

Experimental testing consists of a quasi-static as well as a dynamic characterization. 9 corroded specimens (3 corrosion rates and 3 corrosion configurations) and the reference beam are tested by means of an actuator on the strong floor. The dynamic testing of the 9 other corroded beams (3 corrosion rates and 3 corrosion configurations) in addition to the un-corroded beam is performed on the AZALEE shaking table. The setup is similar to the one used for the IDEFIX campaign [36], except for some modifications designed to adapt the spinning supports for accommodating unusually high range displacements and rotations.

2.4.1. Quasi-static testing

Regarding the quasi-static tests, the corroded and non-corroded beams are subjected to a classical four-point alternate bending test on the TAMARIS strong floor. The loading is applied by means of a long-stroke actuator linked with a reinforced metal beam able through swivels at its ends to distribute the loading on two points of the DYSBAC beam. The actuator of 100 KN capacity has a maximum displacement of $\pm$ 500 mm and a maximum velocity of 1.7 $m.s^{-1}$. A general view on the experimental setup is given in Figure 4.

In this study, a four-point bending test was chosen rather than a three-point bending test to ensure a homogeneous state of stress between the two loading points of the specimen, and to limit shear. Indeed, if three-point bending test had been performed, damage would have resulted from a combination of bending and shear.

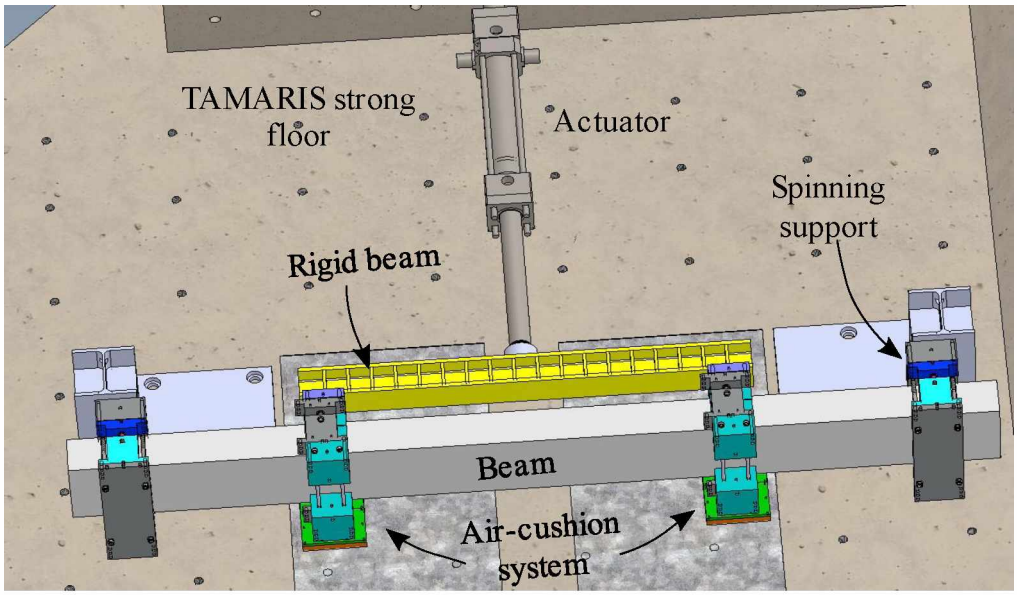

Figure 4: General view of the experimental setup for the quasi-static tests.

2.4.2. Dynamic testing

The dynamic tests are performed on the AZALEE shaking table. It is a 6 × 6 m^2 shaking table able to reproduce seismic signals up to 3 g depending on the payload. The table is controlled on the 6 degrees of freedom (3 rotations, 3 translations) (Figure 5).

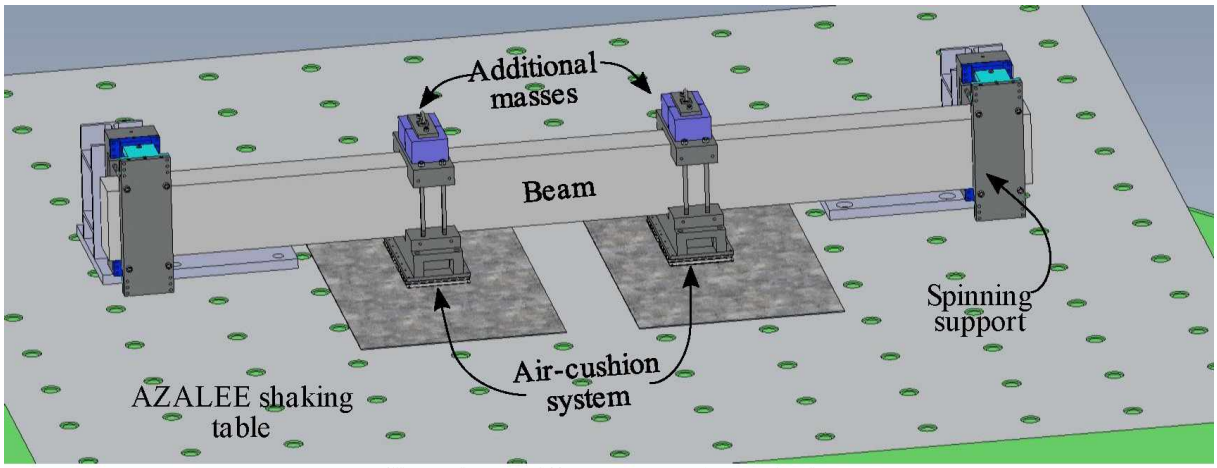

Figure 5: General view of the experimental setup for dynamic tests.

2.4.3. Boundary conditions and additional masses

The specimens are excited for both dynamic and quasi-static tests along their weakest flexural axis with the aim of achieving the failure and to characterize structural responses related to ultimate limit state such as the maximum ductility level. The boundary conditions are the followings:

- spinning supports allowing the rotation at the beam extremities around the vertical axis. These supports are designed to ensure a maximum rotation angle of $\pm 24°$ at the beam boundaries which is consistent with the expected maximal displacement at the loading points of $\pm 400\ mm$ (Figure 4);
- two additional masses of $94\ kg$ weight each, fixed at the intermediate supports. These masses ensure a first natural frequency around $13\ Hz$ within the operating frequency range of AZALEE shaking table. The lumped masses including the intermediate support and the additional masses are around $310\ kg$ each (Figure 5). The initial first eigenfrequency has been designed sufficiently high in order to follow its decrease with respect to the undergone damage;
- two air-cushion systems to bear the beam weight and to drastically reduce the friction between the beam and the shaking table's or strong floor's upper plate. These measures are taken to prevent the beam from cracking under its dead weight in addition to the lumped masses weight (Figure 4 and Figure 5).

2.4.4. Measurements

In order to fully characterize the mechanical response of the specimens during the tests, different types of sensors are used:

- 5 displacement wire sensors;
- 2 high precision displacement wire sensors;
- 2 six-axis load cells at the beam ends;
- 7 three-axis accelerometers.

In addition, the digital image correlation technique (DIC) is used. It consists of painted black and white strips on the upper surface of the beam. The displacement of these strip is followed in time using a stereoscopic system. In this way, the deformed shape of the beam during the tests can be estimated. Figure 6 shows the type and position of the used sensors.

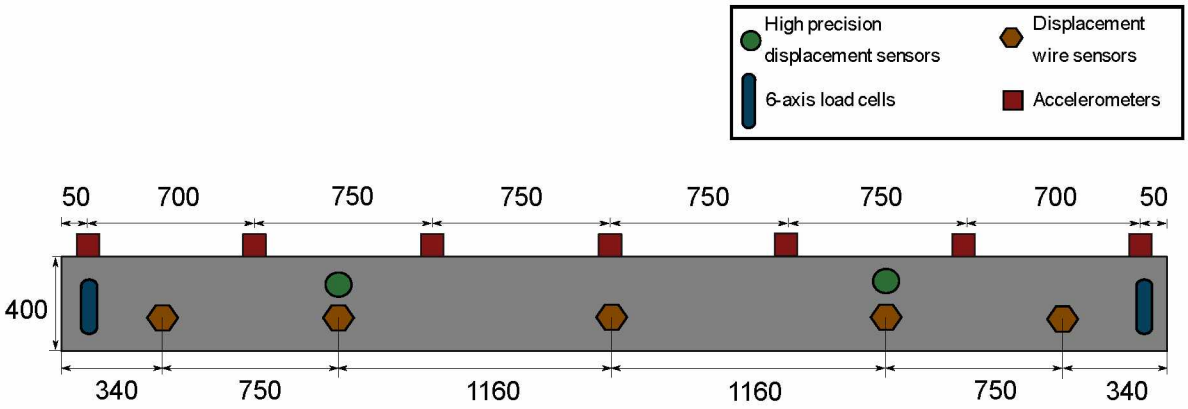

Figure 6: Sensors positions – front view - dimensions in millimeters.

2.5. Loading

2.5.1. Quasi-static loadings

The applied loading is composed of blocks of 3 identical cycles during which displacement is prescribed, with an increasing amplitude between two consecutive blocks (Figure 7). Each cycle involves 4 phases: loading in one direction, unloading, loading in the other direction and unloading. The goal behind having 3 cycles is to stabilize the new damage level of the current block before moving on to the next one. The amplitude range varies from $0.4\ mm$ up to $200\ mm$. The loading velocity is kept constant equal to $0.5\ mm.s^{-1}$.

Hammer shock testing between the blocks is also performed in order to get the evolution of the modal properties with damage. Since hammer shock results, in particular the equivalent viscous damping ratio (EVDR), are sensitive to the test conditions (impact intensity, direction of impact…), all hammer tests have been performed by the same operator all along the experimental campaign.

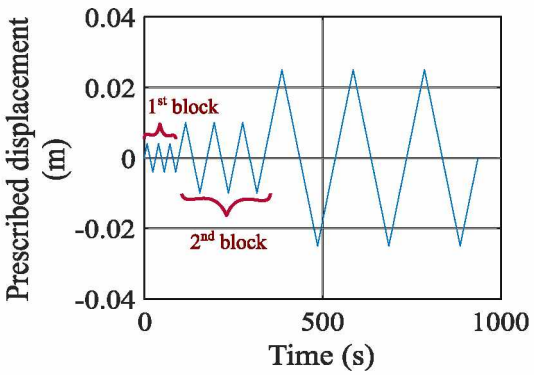

Figure 7: Applied loading in quasi-static testing.

2.5.2. Dynamic loadings

The dynamic loading consists in a synthetic signal able to excite only the first natural mode of the beam. It is a bandlimited signal between 2 and 13 Hz (Figure 8). This choice has been made in order to take into account the frequency shift due the damage growth during the test. Five acceleration levels are used: $0.125\ g$, $0.5\ g$, $0.8\ g$, $1.25\ g$ and $2\ g$. A modal characterization of each beam is performed before testing and between two consecutive testing sequences using a white noise signal ($PGA = 0.1\ g$).

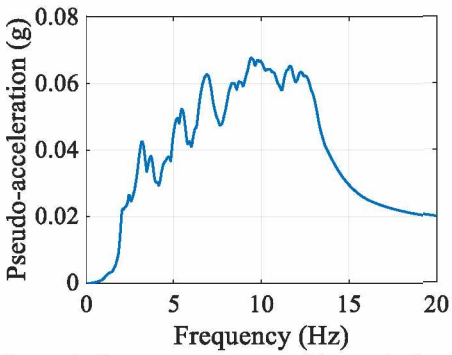

Figure 8: Response spectrum of the applied signal.

3. Corrosion state characterization

3.1. Mass loss measurement

The mass loss rate is difficult to measure experimentally on the tested beams, because of their large dimensions as well as the high reinforcement density. To address this issue, 9 dedicated RC specimens were cast with the same concrete formulation and the same steel reinforcement used for the real tested beams. The specimens of $72 \times 72 \times 4500\ mm^3$ are crossed by a HA12 bar and have a concrete cover thickness equal to the one of the campaign beams (Figure 9). A group of 3 specimens were corroded at 5 %, 3 others at 10 % and the last 3 at 15 % using the same setup as the one presented in section 2.3.

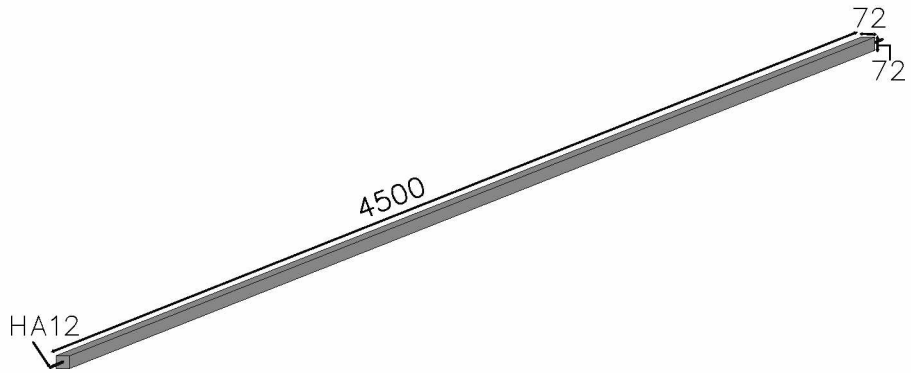

Figure 9: Design of specimens dedicated to measure the actual mass loss - dimensions in millimeters.

The rebars were removed from the concrete and mechanically cleaned afterwards. The objective was to remove the rust products and to weigh the residual steel. The corrosion rate is estimated according to Equation 2.

$$\tau = \frac{M_i - M_f}{M_i} \quad (2)$$

where M_i is the weight of the rebar before the corrosion process and M_f is the residual weight of the rebar after removing the corrosion products.

Table 3 summarizes the mean weighing results. Based on these results, we can notice that the measured corrosion rate is lower than the target ones. This is due to the under-estimation of the α coefficient which is a parameter depending on the concrete porosity and the concentration of chlorides in the solution. It is important to be noted that the initial assumed value of α is taken from some experiments carried out in published studies [15].

Table 3: Mean weighting results.

Target corrosion rate (%)	M_i (g)	M_f (g)	Estimated corrosion rate (%)
5	3966	3841	3.1
10	3966	3716	6.3
15	3966	3592	9.4

3.2. Cross section loss measurement

Since the chloride RC corrosion is not uniform, the mass loss ratio is not a sufficient indicator to characterize the corrosion state. For this reason, using the same bars extracted from the specimens dedicated to the mass loss measurement (see paragraph 3.1), the distribution of the steel cross section diameter has been measured. The measurements have been realized by the means of a profilometer bench with a running transverse laser beam along the bar. This technique makes it possible to measure the diameter with a great precision and to make measurements at very close points, at each one millimeter in this case of study.

Figure 10. a shows the experimental setup and Figure 10. b is an example of the measured diameter distribution for a 10% corroded bar.

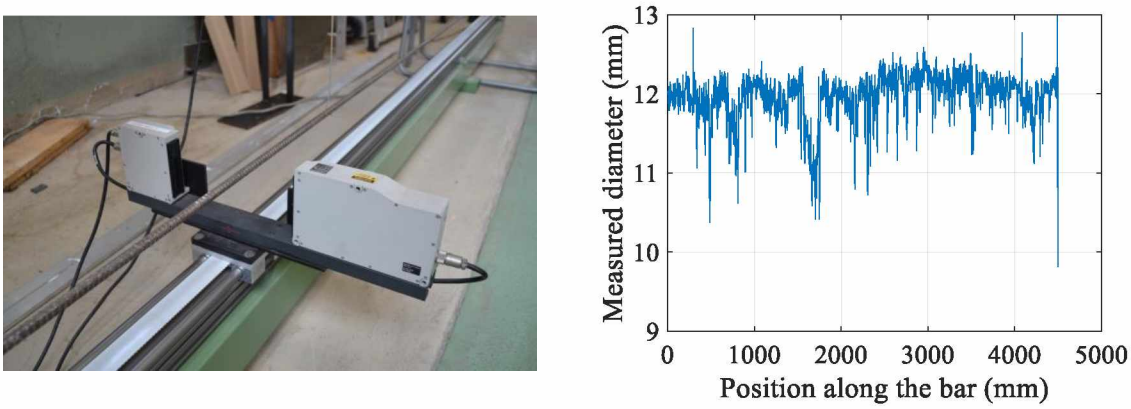

Figure 10 : The cross section loss measurement: (a) the experimental setup, (b) example of a measured diameter distribution.

Figure 11 is a statistical analysis of the measured cross section diameter. Based on these results, a substantial decrease of the measured cross section diameter with the increase of the corrosion degree is observed. Moreover, the frequency of small diameters increases with the increase of the corrosion level.

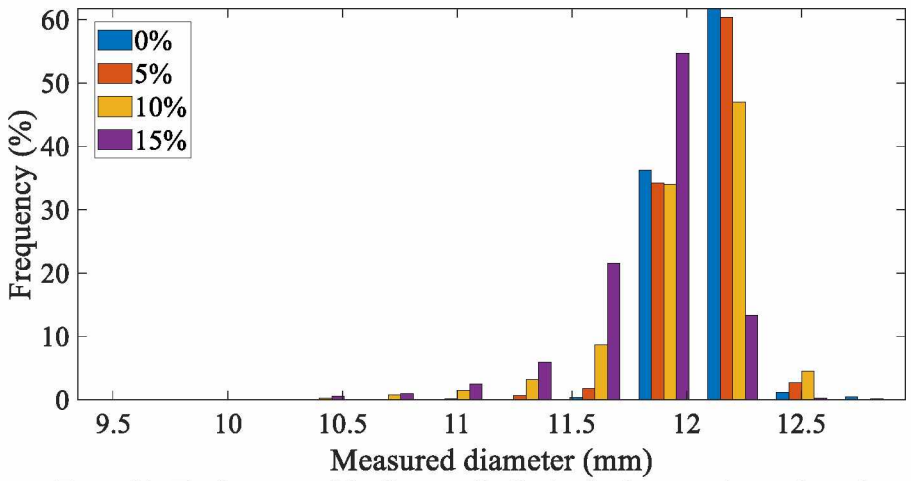

Figure 11 : The frequency of the diameter distribution for the targeted corrosion ratios.

Table 4 summarizes statistical indicators coming from the measured diameter distributions. A decrease of both average and minimum diameter with the increase of corrosion degree can be noticed. The maximum value of the diameter mainly depends on the pits position, which can be in the bar ribbed parts or not.

The standard deviation is an indicator that assesses the measurements dispersion. It can be observed that the more the bar is corroded, the more the diameter distribution is dispersed. These experimental investigations will help one to perform numerical analysis of the experimental campaign for model identification or validation purposes.

Table 4 : Statistical indicators of the measured diameter distributions.

Targeted mass loss (%)	Minimum diameter (mm)	Maximum diameter (mm)	The average diameter (mm)	Standard deviation (mm)
0	11.693	13.555	12.096	0.144
5	10.901	12.598	12.083	0.167
10	9.820	12.983	11.997	0.300
15	9.656	12.766	11.797	0.295

3.3. Steel/concrete interface

In order to characterize the degradation of bond strength between steel and concrete with corrosion, additional specimens were cast.

The pull-out specimen is a concrete cube of $200 \times 200 \times 200\ mm^3$ crossed by a steel bar (HA12 in our case). The steel bar is covered by a tube, generally made of polyvinyl chloride (PVC), to prevent bonding between steel and concrete over a length equal to 5 times the diameter of the bar. The design and casting of these specimens were achieved according to the recommendation of the RILEM association [37].

12 pull-out specimens were cast: 3 of them were kept non-corroded whereas the others were corroded using the technique of corrosion induced by an imposed current at 5%, 10% and 15%. These specimens are tested, according to the method described in [37]: a tensile force is applied to one side of the bar through an hydraulic cylinder (Figure 12). The end slip is measured by a linear variable displacement transducer sensor (LVDT) placed on the unloaded side of the bar.

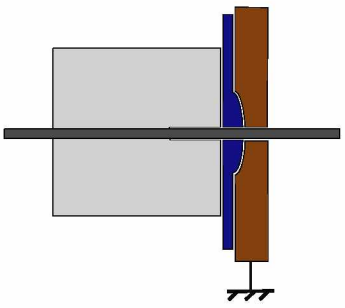

Figure 12: Pull-out experimental setup.

The applied load P is measured by the actuator load cell whereas the displacement is measured by the sensor put on the steel bar edge. The bond strength is calculated by Equation 3.

$$f = \frac{P}{\pi.d.l} \tag{3}$$

where P is the applied load by the actuator, d is the steel bar diameter and l the embedment length of the reinforcement.

The mean results in terms of ultimate bond strength and rebar slip for the corroded and non-corroded specimens are presented in Table 5. The maximum rebar slip corresponds to a total loss of bond between

steel and concrete. Based on these results, we can notice an increase of the ultimate bond strength and a decrease of the rebar slip in the early stages of reinforcement corrosion (5 % and 10 % targeted corrosion rates). For the target corrosion rate of 15 %, a brutal decrease of the ultimate bond strength and in the rebar slip as well is observed. These results are consistent with previous studies dealing with the effect of corrosion on bond-strength [32].

Table 5: Mean results of the carried out pull-out tests.

Corrosion rate (%)	Ultimate bond strength (MPa)	Maximum rebar slip (mm)
0	6.2	28.06
5	8.6	20.79
10	8.2	17.72
15	2.4	6.09

4. Experimental Results and discussion

In this section, the experimental results are presented and discussed. The quasi-static and dynamic testing results are presented and cross-checked in order to reveal the similarities and the potential differences. It is to be noted that the C3_15% beam is excluded from the results discussion. This is due to an incident that occurred during the corrosion process, making the experimental results incomparable with the other configurations and corrosion rates.

4.1. Capacity and hysteretic curves

The capacity curve is one of the first interesting indicators to assess the structural performance of RC structures. In this paragraph, capacity curves are extracted for the different beam configurations and corrosion degrees from both quasi-static and dynamic testing.

The hysteretic curves are an interesting tool that reveals the ability of a structure to dissipate more or less energy. The hysteretic curves have been extracted from both quasi-static and dynamic tests for the non-corroded specimen in addition to the C_1 corroded beams.

The objective is twofold and consists in highlighting the effect of the corrosion (configuration and corrosion rate) on structural response of corroded RC members as well as comparing the trends revealed by both types of testing.

4.1.1. Quasi-static testing condition

Figure 13 depicts the cyclic force-displacement curves for the non-corroded beam and the three C_1 corroded specimens. The force considered is the sum of the reactions measured on each beam support in the direction of the force application, whereas the displacement is measured at mid-span.

From Figure 13, the hysteretic capacity is analyzed. A decrease of the loop area is observed at each prescribed displacement level with an increasing corrosion degree. This result is consistent with what was revealed by other studies in the literature [18] [20].

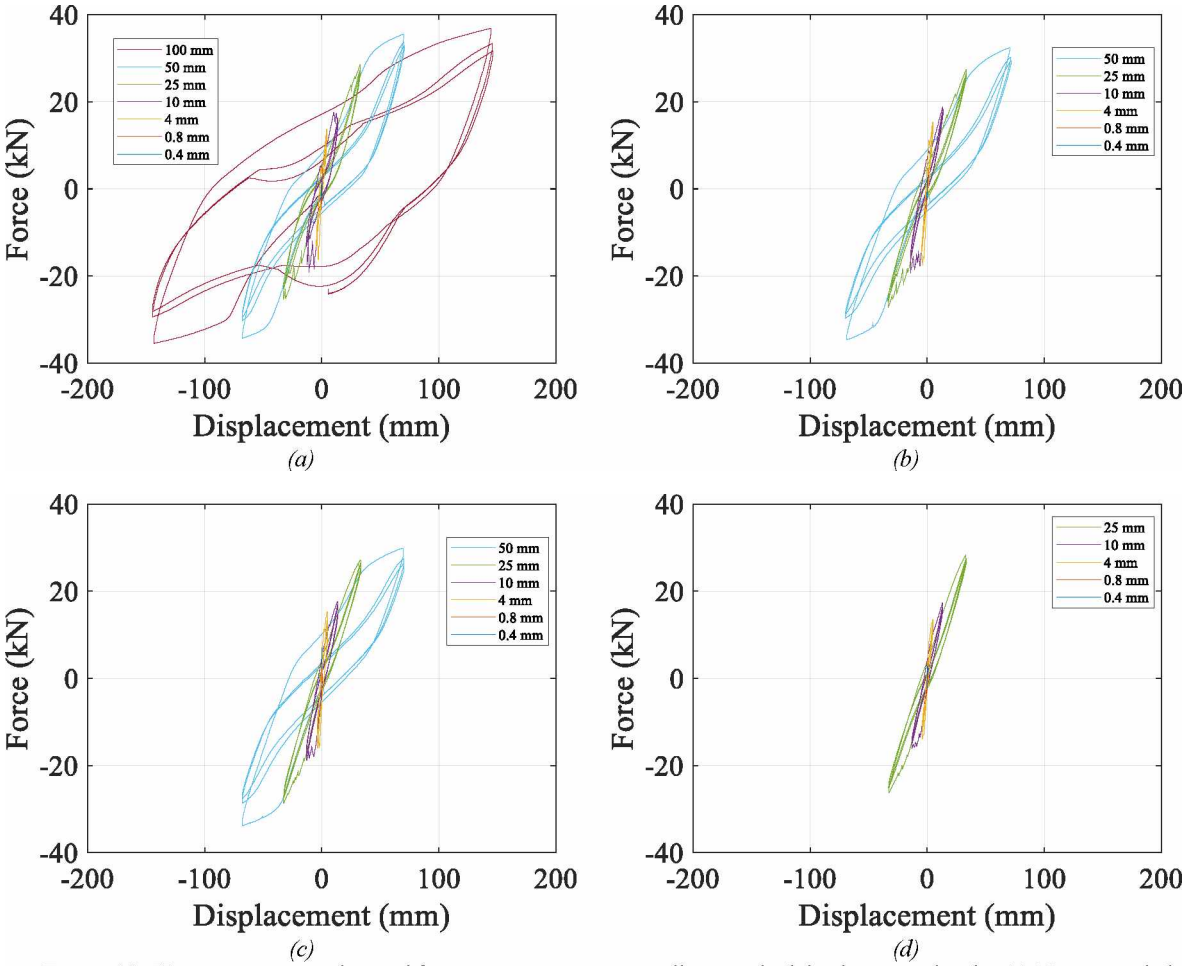

Figure 13: Hysteretic curves obtained from quasi-static tests at all prescribed displacement levels: (a) Non-corroded specimen, (b) C1_5 specimen, (c) C1_10 specimen, (d) C1_15 specimen.

The capacity curves are obtained by considering the envelope of the force-displacement responses. The capacity curves obtained through the cyclic quasi-static loads is similar to the one resulting from a pushover analysis, assuming that the compressed cracked concrete fully regains its initial properties when the cracks are closed. Only the loading phase is considered in each block. The results are shown in Figure 14 .

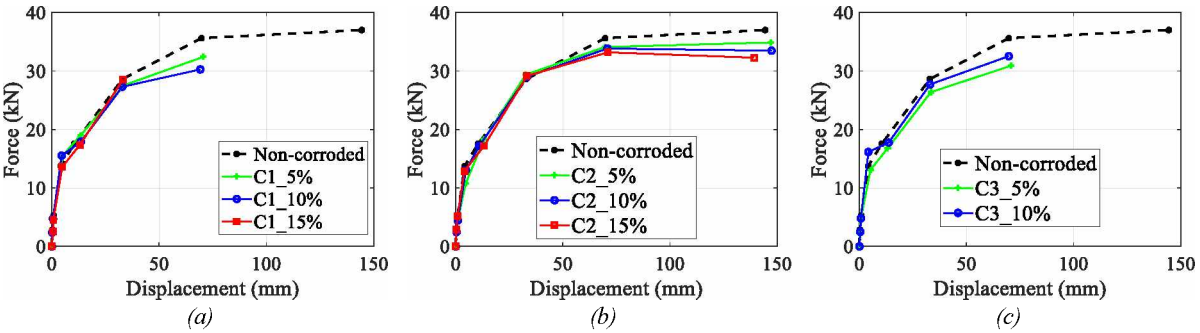

Figure 14: Capacity curves obtained from quasi-static tests: (a) C_1 configuration, (b) C_2 configuration, (c) C_3 configuration.

For the C_1 specimens, a decrease of the capacity and the maximum measured displacement is observed with respect to the non-corroded beam with an increasing corrosion degree. The bearing capacity of the un-corroded beam is decreased by 12%, 18% and 23% for the C1 corroded beams at 5%, 10% and 15% respectively. This decrease is even more significant (51%, 52% and 77%) regarding the maximum

measured displacement for the same beams. It is to be noted that the failure of the tested specimens is governed by bending, as illustrated in Figure 15.

For the C_2 configuration, the corroded beams exhibit almost the same capacity as the non-corroded one. This can be explained by the fact that stirrups do not provide bending stiffness.

Regarding the C_3 configuration, the corroded beams show a decrease of the capacity as well as the maximum measured displacement with respect to the non-corroded one. The obtained results are in good agreement with the ones presented in different studies reported in the literature [3].

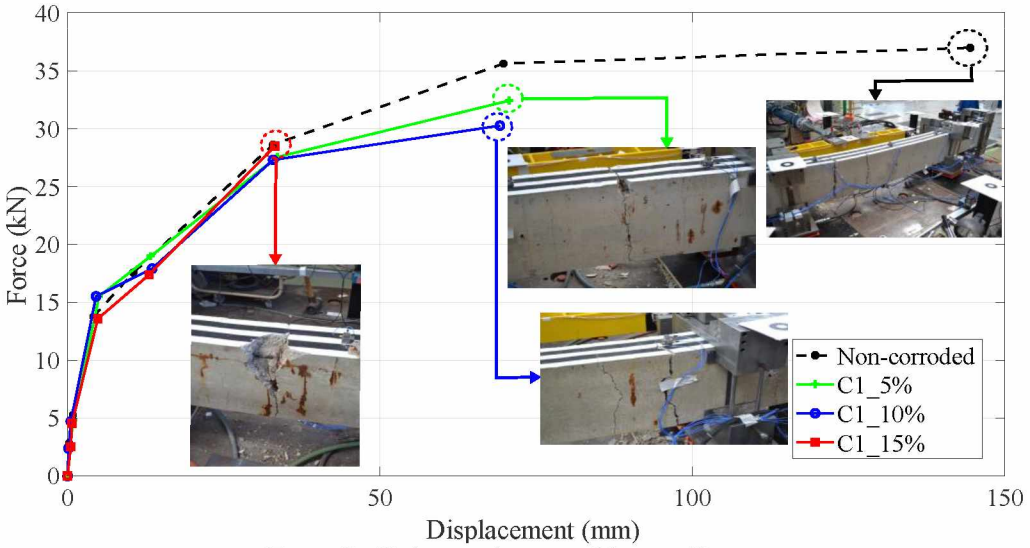

Figure 15: Failure mechanisms of the tested beams.

4.1.2. Dynamic testing condition

Thanks to the measurements carried out during the dynamic testing, the force-displacement curves are obtained. Figure 16 depicts the force-displacement curves for the non-corroded beam and the three C_1 corroded specimens. The force considered is the sum of the reactions measured on each beam support in the direction of the force application, whereas the displacement is measured at mid-span.

Based on Figure 16, it can be noticed a decrease in the global displacement capability of the specimen with an increasing corrosion degree. Furthermore, the force-displacement loop at a given excitation level becomes narrower with an increasing corrosion rate. This result is consistent with what was revealed during the quasi-static tests (see paragraph 4.1.1) as well as a previous experimental campaign using dynamic loadings [21].

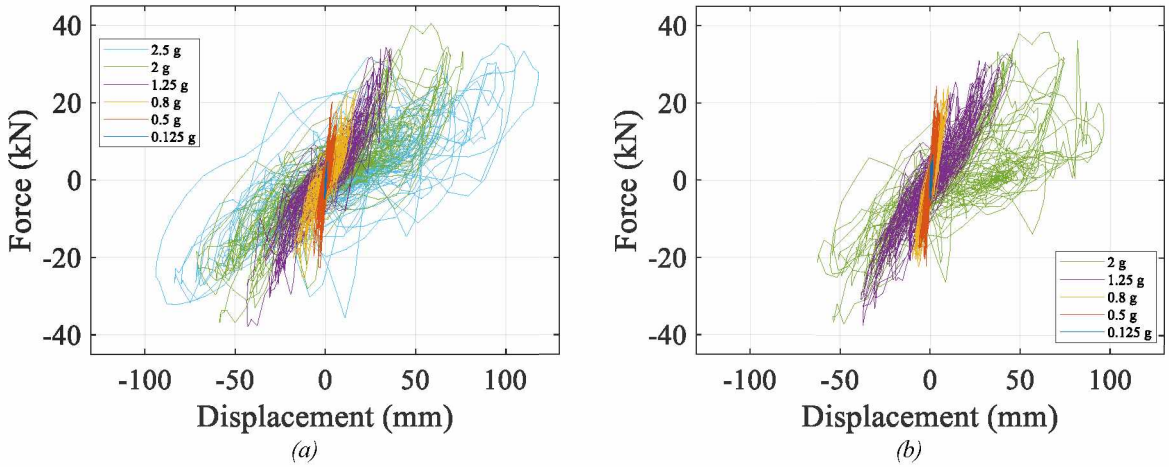

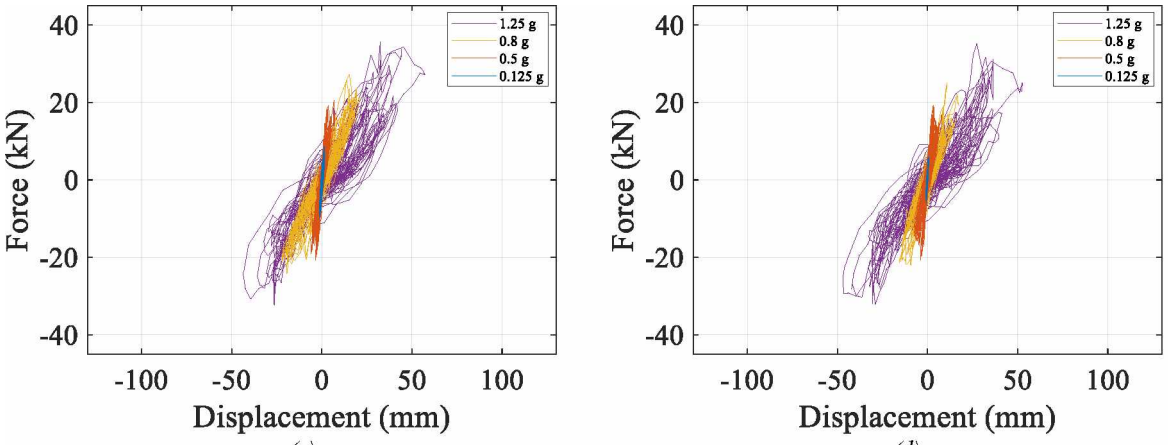

Figure 16: Force-displacement curves obtained from dynamic tests at all applied PGA levels: (a) Non-corroded specimen, (b) C1_5 specimen, (c) C1_10 specimen, (d) C1_15 specimen.

The obtained capacity curves from dynamic tests are plotted in Figure 17. The same observations as the capacity curves obtained from quasi-static testing can be made (see paragraph 4.1.1). It is important to notice that the curve trends obtained from both types of testing are comparable, which is not the case for the numerical values. This might be due to the difference between the loading nature (quasi-static/dynamic) used in each testing type.

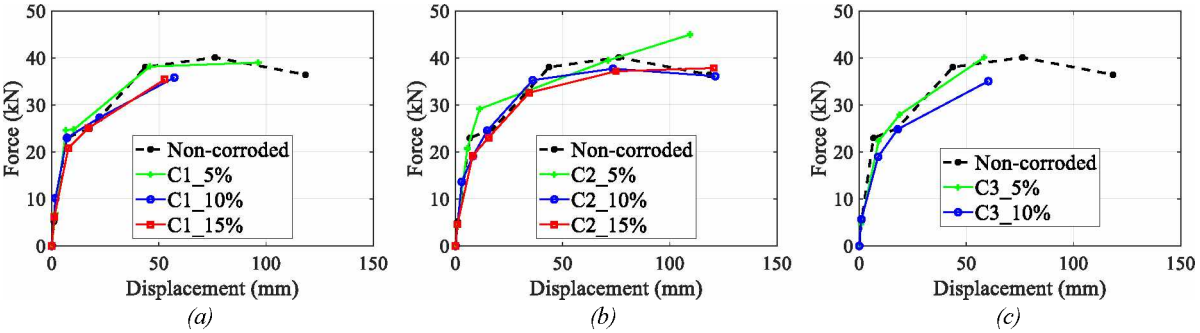

Figure 17: Capacity curves obtained from dynamic tests: (a) C_1 configuration, (b) C_2 configuration, (c) C_3 configuration.

4.2. Ductility offer evolution

The ductility offer is an indicator that measures the ability of a structure to accommodate the loading without compromising the structural integrity. In earthquake engineering, a high ductility offer denotes a great ability of the structure to deform and therefore, to dissipate energy without reaching ultimate failure. The maximum ductility ratio was determined during the DYSBAC experimental campaign for each beam configuration and corrosion rate for both quasi-static and dynamic testing. The ductility ratio is defined according to Equation 4:

$$\mu = \frac{\max|u(t)|}{u_y} \tag{4}$$

where $\max|u(t)|$ is the maximum of the absolute value of the relative displacement measured at midspan with respect to the supports, and u_y is the midspan displacement corresponding to the first yield occurrence in the beam steel rebars. It is determined based on the appearance of a residual measured displacement along the beam.

4.2.1. *Quasi-static testing condition*

Figure 18 depicts the evolution of the maximum ductility ratio with respect to targeted corrosion degree.

Based on Figure 18, it is observed that for the C_1 beams, an increase in the corrosion degree leads to a decrease of the maximum ductility ratio. This can be explained by the degradation of the steel mechanical properties, namely the ductility, as reported in many previous studies [35] [2].

For the C_3 configuration beams also, an increase in the corrosion severity leads to a decrease in the ductility ratio. This observation is consistent with the fact that increasing corrosion induces a decrease in the steel bars ductility [35].

As far as the C_2 configuration is concerned, no noticeable difference in the maximum ductility ratio is revealed with the increase of the corrosion degree. This experimental finding was expected because the transverse reinforcement does not affect the flexural ductility. The minor differences in the measured ductility ratios may be due to the variability usually observed in the material parameters, particularly concrete and the slight differences in the dimensions of the reinforcement cages.

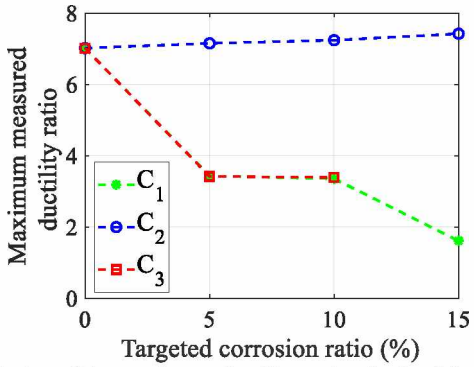

Figure 18: Evolution of the maximum ductility ratio obtained from quasi-static tests.

4.2.2. *Dynamic testing condition*

For the dynamic testing, the maximum ductility ratio was calculated for each tested specimen at the final acceleration level. One can notice that the failure of some beams could not be reached due to the limitations of the shaking table in terms of the maximum allowed displacement and velocity. Figure 19 shows the evolution of the maximum ductility ratio as a function of the targeted corrosion rate.

We can notice that the same trends are revealed in both quasi-static and dynamic testing. For the C_1 and C_3 corroded beams, a decrease in the ductility ratio is observed with the increase of the corrosion degree. As far as the C_2 configuration is concerned, the ductility ratio of the different beams is similar to the reference one. This result was expected since the stirrups does not contribute in the flexural ductility. These observations are fully consistent with respect to the results coming from the quasi-static testing in paragraph 4.2.1.

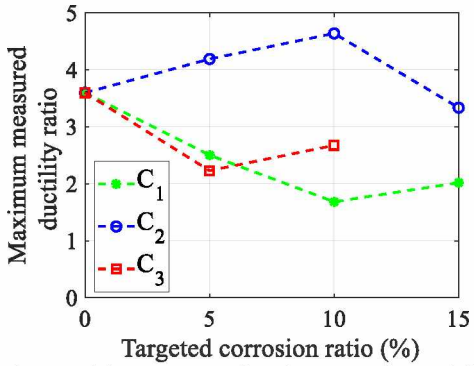

Figure 19: Evolution of the maximum ductility ratio obtained from dynamic tests.

4.3. Eigenfrequency evolution

The decrease of the eigenfrequencies during an excitation is a great indicator of the increase of damage in the structure [38]. For this reason, the evolution of the eigenfrequencies has been followed by hammer tests (for quasi-static loading) and white noise signal (for dynamic loading) after each excitation level.

The hammer shock tests were performed after each prescribed displacement block after disassembling the rigid beam to which the actuator was connected. The objective was to keep the same boundary conditions as the ones considered in the dynamic testing. The hammer tests were done only till the steel yielding because of the technical difficulty to connect again the rigid beam to the concrete beam when the latter is permanently deformed. Given the fact that after the steel yielding the degradation of the eigenfrequencies is not significant, this choice is fully justified.

The white noise signal, which is a random signal having equal intensity at different frequencies, is applied by the means of the shaking table after each acceleration level. In our case, the frequencies considered to generate this type of signal are between 0.5 Hz and 40 Hz. Given the fact that the theoretical initial 1st and 2nd eigenfrequencies are respectively around 13 and 36 Hz, the determination of the two first eigenfrequencies was possible. Because the specimens exhibit a behavior that mostly includes bending, only the first eigenfrequency is analyzed. However, the acquired data allow a similar analysis for the second eigenfrequency to be performed if needed.

4.3.1. Hammer shock tests

When performing hammer shock tests, the beam is excited along its weakest flexural axis in two locations: at midspan (in order to get symmetrical modes) and at the quarter-beam (for the non-symmetrical modes). Then, the frequency response function (FRF) is calculated for each accelerometer. The observed peak corresponds to an eigenfrequency of the beam. The midspan accelerometer is used to determine the 1st eigenfrequency. The evolutions of the 1st eigenfrequency with respect to the maximum prescribed displacement (in absolute value) related to the last applied loading block for the different tested beams are plotted in Figure 20. In this figure, the imposed displacement level leading to the steel yielding is presented in dashed lines.

Based on Figure 20, at the same prescribed displacement level, the corroded beams are characterized by a higher eigenfrequency with respect to the no corroded one. This observation may be explained by the enhancement of the bond strength at the steel/concrete interface (paragraph 3.3). Paradoxically, the corroded beams are more damaged than the reference beam at the same displacement level, as shown by the capacity curves presented in paragraph 4.1. Consequently, the eigenfrequency seems to be an unreliable damage indicator in the case of RC structures affected by a low corrosion level.

If we focus on the level of damage of each beam at the time of steel yielding, we can compare the 1st eigenfrequency identified for each beam and consider it as an indicator of the structural damage level. In case of the C_1 configuration, we can notice that the steel yielding phase for the 10 % and 15 % corroded beam is characterized by a 1st eigenfrequency around 6 Hz, whereas in case of the beam with a corrosion rate of 5 % and the non-corroded one, yielding occurs when the 1st eigenfrequency is around 3 Hz (see Figure 20. a). This observation is consistent with the results regarding the ductility offer presented in paragraph 4.2.

The C_2 configuration beams undergo the steel yielding at the same imposed displacement level as the one applied in case of the non-corroded beam. At this yielding stage, the first eigenfrequency of these beams is around 3 Hz. The steel yielding for the 5 % and 10 % C_3 corroded beams occurs when the 1st measured eigenfrequency is around 5 Hz.

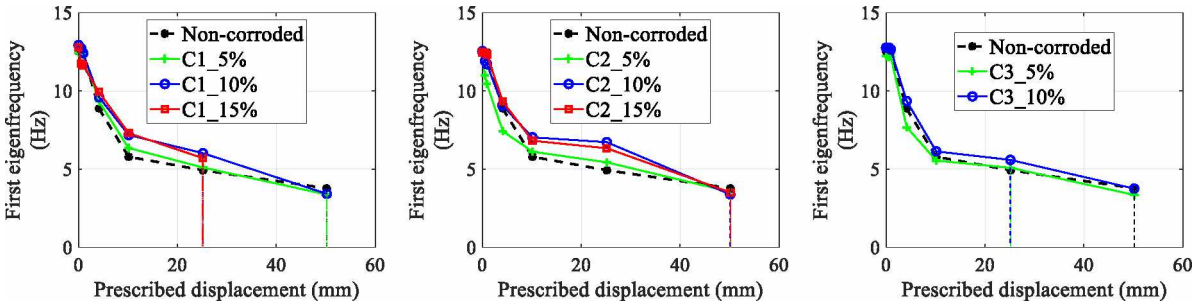

Figure 20: Evolution of first eigenfrequency obtained from quasi-static tests: (a) C_1 configuration, (b) C_2 configuration, (c) C_3 configuration.

4.3.2. White noise tests

During the dynamic testing, a white noise (WN) signal is applied along the weakest flexural axis of each beam after each applied acceleration level. A first advantage of this type of tests, compared with the hammer shock tests, lies in the fact that the same excitation level is applied to the specimens. A second advantage is that there is no need to change the assembly before applying the desired signal whereas this has to be done in case of hammer shock tests. Therefore, the analyses were done up to the loading block prior to failure for the beams having experienced failure, and include the last dynamic test for the beams for which failure could not be reached. The eigenfrequencies of each beam related to each acceleration level are determined by the detection of the FRF peaks.

In Figure 21, the 1st eigenfrequency evolutions for the different tested beams are plotted in function of the realized PGA measured on the shaking table upper plate during the previous applied acceleration level. No major differences were noted regarding the 1st natural frequency drop-off identified for the different specimens. The results obtained regarding the 1st eigenfrequencies identified after the steel yielding phase for the different tested beams are consistent with the results coming from hammer shock tests and presented in in paragraph 4.3.1.

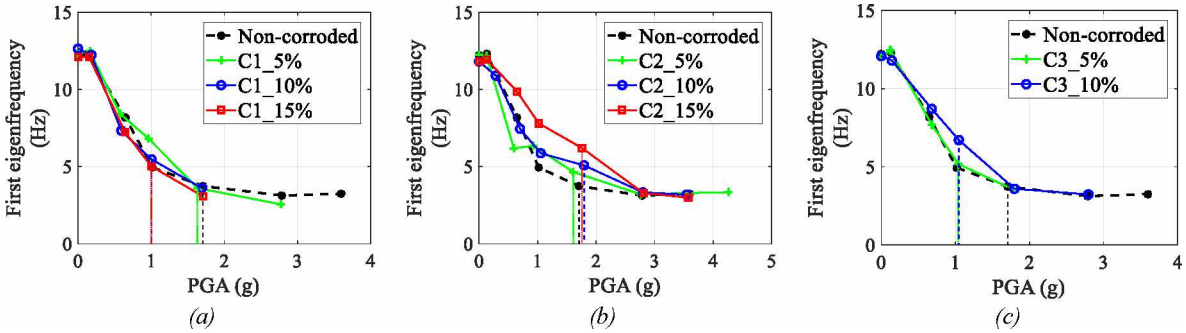

Figure 21: Evolution of first eigenfrequency with respect to the realized PGA identified from dynamic tests: (a) C_1 configuration, (b) C_2 configuration, (c) C_3 configuration.

4.4. Damping ratio evolution

Thanks to the hammer shock tests performed during the quasi-static campaign as well as the WN tests during the dynamic campaign, we were able to identify the modal damping ratio. Many methods can be used to estimate the modal damping ratios, in particular the half-power bandwidth method [39]. This method is particularly suitable when low level excitations are considered [39]. Therefore, this technique was applied to the data coming from hammer shock and low intensity white noise tests. In this method, the system is assumed to be a linear viscously damped single degree of freedom system (SDOF), subjected to a mono-harmonic loading. Equation 5 can be used to identify the modal damping ratio. The reader can refer to [39] for more details.

$$\xi = \frac{\omega_2 - \omega_1}{2.\omega_r} \qquad (5)$$

where ω_r is the eigenfrequency, ω_1 and ω_2 are the half-power frequency points. If we note X the FRF, $|X(\omega_r)| = |X(\omega)|_{max}$ and $|X(\omega_1)| = |X(\omega_2)| = \frac{|X(\omega)|_{max}}{\sqrt{2}}$.

4.4.1. *Hammer shock tests*

The 1st modal damping ratios identified from the hammer shock tests are presented in Figure 22 for the different specimens. We can notice that for all the tested specimens, the damping ratio increases during the first displacement blocks then remains almost constant.

For all the tested beams, the corroded beams are less damped compared to the reference one for all applied displacement level. This observation was not expected since the cracking induced by corrosion in the concrete cover should increase the damping by the friction between cracks. In [18], the authors performed an experimental campaign on cantilever piers by considering cyclic loadings. The corresponding damping ratios were calculated using the results of the cyclic tests as the ratio between the dissipated energy and the elastic one. The results show that the corroded specimens are characterized by a higher damping ratio than the un-corroded one in contrast with the results obtained with hammer shock testing during DYSBAC experimental campaign. The identified differences between the two studies are probably due to the nature of the hammer test itself, which relies on a local excitation of the specimen. In this case, not all the damping mechanisms are activated and the damping ratio is underestimated. The use of WN identification considering a dynamic situation (following section), implying a complete inertial loading of the specimen helps one to better measure this evolution of damping ratio with the level of degradation.

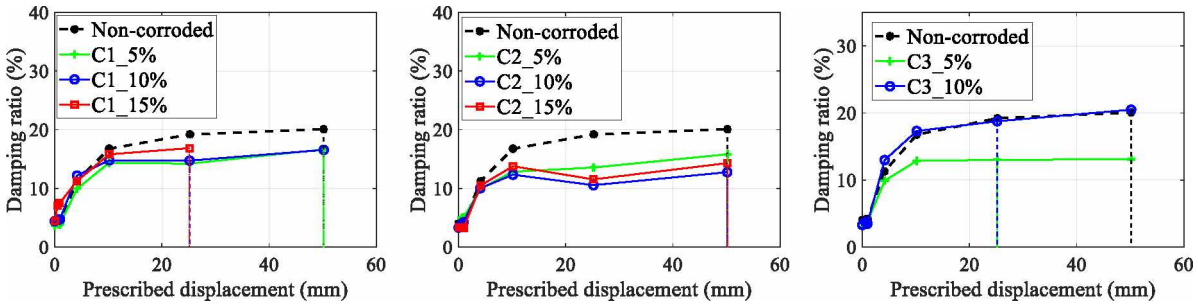

Figure 22: Evolution of first damping ratio obtained from quasi-static tests: (a) C_1 configuration, (b) C_2 configuration, (c) C_3 configuration.

4.4.2. *White noise signal*

The 1st modal damping ratios after each PGA level for all the tested beams were identified using the half-bandwidth method applied on the data coming from WN tests. Figure 23 depicts the relationship between the identified modal damping ratios and the PGA of the applied signal.

For the C_1 configuration, we can notice that the 5 % corroded beam is more damped compared to the reference beam, both before and after the steel yielding phase. The 10 % and 15 % corroded beams are characterized by a higher damping ratio at each acceleration level before the steel yielding. After this stage, the damping ratio of the corroded beams decreases below the value identified in case of the reference beam. This observation is consistent with the fact that the 5 % corroded beam is characterized by a better concrete-steel interface compared with the non-corroded one [32]. This enhancement is due to the corrosion products that fill the pores between steel and concrete without damaging the concrete cover. After the steel yielding, the damping is related to the rebars behavior. Knowing that the steel ductility decreases with the increase of the corrosion degree, the behavior of the beams C1_10 and C1_15, after the yielding, are fully understandable.

For the C_2 configuration, the evolution of the damping ratio identified in case of corroded specimens is almost similar to the reference beam. These results are consistent with all the inspected aspects in this part (ductility offer, capacity and eigenfrequency) where similarities between the behavior of the corroded C2 beams and the non-corroded one are unarguable.

Regarding the fully corroded beams (C_3 configuration), the 5 % and 10 % corroded beams are more damped for low and intermediate applied PGA (up to 1.25 g). For the high acceleration levels and after the steel yielding, the modal damping ratio decreases more in comparison with the un-corroded beam. This may be explained by the fact that before the steel yielding the cracks induced by corrosion in the concrete cover dissipate the input energy; hence the damping capacity is higher for the C_3 beams compared to the non-corroded beam. After the yielding, the steel ductility is the only parameter that drives the damping capacity, this parameter is reduced for the corroded beams. These results are in a good agreement with the conclusions drawn by [21].

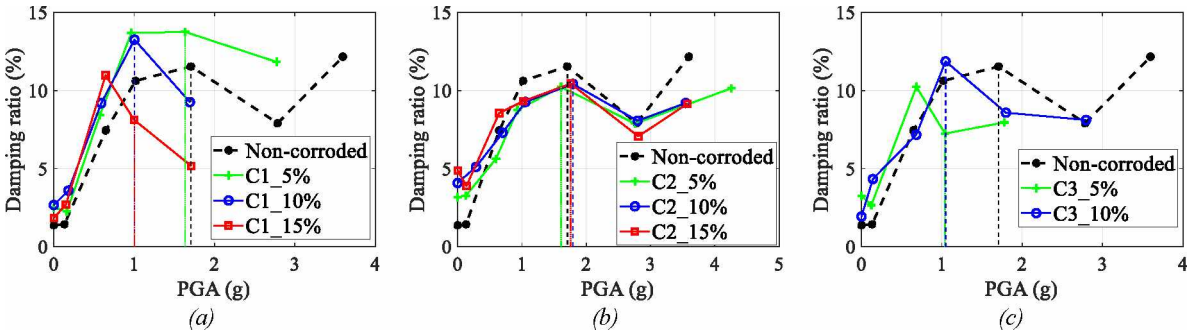

(a) (b) (c)

Figure 23: Evolution of first damping ratio obtained from dynamic tests: (a) C_1 configuration, (b) C_2 configuration, (c) C_3 configuration.

5. Conclusions

In this paper, the results and conclusions from an extensive experimental campaign aiming at assessing the influence of corrosion on both the dynamic and the static properties of RC members have been presented.

In this study, some well-known facts in the literature about corroded structures are consolidated. Lightly corroded specimens show an increase in the ultimate bond strength and a decrease in the maximum rebar slip compared with the un-corroded specimen. On the contrary, a brutal drop-off in the bar slip and the ultimate bond strength is observed for the highly corroded specimens.

The performed statistical analysis of the diameter distributions for the corroded bars shows a decrease in the average and minimum diameter with the increase of the corrosion degree. For the highly corroded bars, the diameter distribution is more dispersed compared with the lightly corroded bars.

The comparison between the findings coming from quasi-static and dynamic testing, which is one of the original contributions of the present study, leads to a good concordance of conclusions regarding the quasi-static properties (the bearing capacity, the hysteric response and the maximum ductility). The longitudinal corroded beams C_1 as well as the fully corroded C_3 beams display a degradation in quasi-static characteristics compared with the reference beam. Whereas, the corrosion of stirrups, in the C_2 beams, has little influence on the bending response of corroded members.

The dynamic properties, in particular the 1st eigenfrequency as well as the damping ratio, are determined based on experimental data obtained by hammer shock and white noise tests. The corroded specimens are characterized by higher eigenfrequencies than the reference beam, at each displacement level, despite of more observed damage. Thus, the eigenfrequency is an unreliable damage indicator for lightly corroded RC elements. The two testing methods (hammer shock and white noise) stand together on this finding. Regarding the damping ratio, the evolutions identified from white noise tests are more relevant

compared with the ones coming from hammer shock tests. Identification under dynamic configuration should thus be chosen in the dynamic inspection of corroded RC members.

The next step of this study is to investigate more complex identification methods used to evaluate some major aspects related to the dissipation energy and the damping capability, as has been done for previous shaking table tests on uncorroded beams [36]. The main purpose is to compare the conclusions drawn from dynamic and quasi-static tests based on these complex processing ways. Henceforth, a non-linear numerical model, combining the corrosion pathology effects (using a probabilistic approach) and mechanical loadings (quasi-static cyclic / dynamic) can be developed and validated based on the experimental campaign measurements [40].

Acknowledgements

The French Institute for Radioprotection and Nuclear Safety (IRSN) and the Nuclear Energy Division of the French Sustainable Energies and Atomic Energy Commission (CEA/DEN) are kindly thanked for financial supports.

References

[1] H. Böhni, *Corrosion in reinforced concrete structures*. Elsevier, 2005.
[2] J. Sheng et J. Xia, « Effect of simulated pitting corrosion on the tensile properties of steel », *Construction and Building Materials*, vol. 131, p. 90-100, 2017.
[3] M. Maslehuddin, I. A. Allam, G. J. Al-Sulaimani, A. Al-Mana, et S. N. Abduljauwad, « Effect of rusting of reinforcing steel on its mechanical properties and bond with concrete », *Materials Journal*, vol. 87, n° 5, p. 496-502, 1990.
[4] F. Paradis, « Influence de la fissuration du béton sur la corrosion des armatures : caractérisation des produits de corrosion formés dans le béton », PhD Thesis, *Laval University*, 2009.
[5] S. Altoubat, M. Maalej, et F. U. A. Shaikh, « Laboratory Simulation of Corrosion Damage in Reinforced Concrete », *International Journal of Concrete Structures and Materials*, vol. 10, n° 3, p. 383-391, sept. 2016.
[6] Y. Yuan, Y. Ji, et S. P. Shah, « Comparison of two accelerated corrosion techniques for concrete structures », *ACI Structural Journal*, vol. 104, n° 3, p. 344, 2007.
[7] T. Vidal, A. Castel, et R. François, « Analyzing crack width to predict corrosion in reinforced concrete », *Cement and Concrete Research*, vol. 34, n° 1, p. 165-174, janv. 2004.
[8] J. Xu, L. Jiang, W. Wang, et Y. Jiang, « Influence of CaCl2 and NaCl from different sources on chloride threshold value for the corrosion of steel reinforcement in concrete », *Construction and Building Materials*, vol. 25, n° 2, p. 663-669, févr. 2011.
[9] T. El Maaddawy, K. Soudki, et T. Topper, « Long-term performance of corrosion-damaged reinforced concrete beams », *ACI Structural Journal*, vol. 102, n° 5, p. 649, 2005.
[10] A. Traetteberg, V. S. Ramachandran, et P. E. Grattan-Bellew, « A study of the microstructure and hydration characteristics of tricalcium silicate in the presence of calcium chloride », *Cement and Concrete Research*, vol. 4, n° 2, p. 203-221, 1974.
[11] W. Zhu et R. François, « Corrosion of the reinforcement and its influence on the residual structural performance of a 26-year-old corroded RC beam », *Construction and Building Materials*, vol. 51, p. 461-472, janv. 2014.
[12] C. Andrade, C. Alonso, et F. J. Molina, « Cover cracking as a function of bar corrosion: Part I-Experimental test », *Materials and Structures*, vol. 26, n° 8, p. 453-464, oct. 1993.
[13] T. A. El Maaddawy et K. A. Soudki, « Effectiveness of impressed current technique to simulate corrosion of steel reinforcement in concrete », *Journal of materials in civil engineering*, vol. 15, n° 1, p. 41-47, 2003.
[14] G. Mancini, F. Tondolo, L. Iuliano, et P. Minetola, « Local reinforcing bar damage in r.c. members due to accelerated corrosion and loading », *Construction and Building Materials*, vol. 69, p. 116-123, oct. 2014.
[15] A. Meda, S. Mostosi, Z. Rinaldi, et P. Riva, « Experimental evaluation of the corrosion influence on the cyclic behaviour of RC columns », *Engineering Structures*, vol. 76, p. 112-123, oct. 2014.

[16] G. Malumbela, P. Moyo, et M. Alexander, « Behaviour of RC beams corroded under sustained service loads », *Construction and Building Materials*, vol. 23, n° 11, p. 3346-3351, nov. 2009.
[17] Q. T. Nguyen, « Etudes expérimentale et théorique de l'effet de la corrosion sur la fissuration du béton et le comportement global des structures en béton armé », PhD Thesis, Paris 6, 2006.
[18] A. Guo, H. Li, X. Ba, X. Guan, et H. Li, « Experimental investigation on the cyclic performance of reinforced concrete piers with chloride-induced corrosion in marine environment », *Engineering Structures*, vol. 105, p. 1-11, déc. 2015.
[19] H.-S. Lee, T. Kage, T. Noguchi, et F. Tomosawa, « An experimental study on the retrofitting effects of reinforced concrete columns damaged by rebar corrosion strengthened with carbon fiber sheets », *Cement and Concrete Research*, vol. 33, n° 4, p. 563-570, avr. 2003.
[20] Y. Ma, Y. Che, et J. Gong, « Behavior of corrosion damaged circular reinforced concrete columns under cyclic loading », *Construction and Building Materials*, vol. 29, p. 548-556, avr. 2012.
[21] W. Yuan, A. Guo, W. Yuan, et H. Li, « Shaking table tests of coastal bridge piers with different levels of corrosion damage caused by chloride penetration », *Construction and Building Materials*, vol. 173, p. 160-171, 2018.
[22] D. J. Zou, T. J. Liu, et G. F. Qiao, « Experimental investigation on the dynamic properties of RC structures affected by the reinforcement corrosion », *Advances in structural engineering*, vol. 17, n° 6, p. 851-860, 2014.
[23] H. A. Razak et F. C. Choi, « The effect of corrosion on the natural frequency and modal damping of reinforced concrete beams », *Engineering Structures*, vol. 23, n° 9, p. 1126-1133, 2001.
[24] W. H. Mosley, R. Hulse, et J. H. Bungey, *Reinforced concrete design: to Eurocode 2*. Macmillan International Higher Education, 2012.
[25] M. N. Fardis, *Seismic design, assessment and retrofitting of concrete buildings: based on EN-Eurocode 8*, vol. 8. Springer Science & Business Media, 2009.
[26] AFNOR Group, « Steel for the reinforcement of concrete – weldable reinforcing steel – General ». 2005.
[27] Z. P. Bazant, « Physical model for steel corrosion in concrete sea structures-theory », *ASCE J Struct Div*, vol. 105, n° 6, p. 1137-1153, 1979.
[28] S. Caré et A. Raharinaivo, « Influence of impressed current on the initiation of damage in reinforced mortar due to corrosion of embedded steel », *Cement and Concrete Research*, vol. 37, n° 12, p. 1598-1612, déc. 2007.
[29] J. Ožbolt, E. Sola, et G. Balabanić, « Accelerated Corrosion of Steel Reinforcement in Concrete: Experimental Tests and Numerical 3D FE Analysis », in *CONCREEP 10*, 2015, p. 108-117.
[30] S. Coccia, S. Imperatore, et Z. Rinaldi, « Influence of corrosion on the bond strength of steel rebars in concrete », *Materials and structures*, vol. 49, n° 1-2, p. 537-551, 2016.
[31] Y. Auyeung, P. Balaguru, et L. Chung, « Bond behavior of corroded reinforcement bars », *Materials Journal*, vol. 97, n° 2, p. 214-220, 2000.
[32] A. A. Almusallam, A. S. Al-Gahtani, et A. R. Aziz, « Effect of reinforcement corrosion on bond strength », *Construction and building materials*, vol. 10, n° 2, p. 123-129, 1996.
[33] « Projet APPLET : Durée de vie des ouvrages en béton : Approches prédictives performantielles et probabilistes », Project Report, 2006.
[34] A. Ouglova, « Etude du comportement mécanique des structures en béton armé atteintes par la corrosion », PhD Thesis, Cachan, Ecole normale supérieure, 2004.
[35] A. A. Almusallam, « Effect of degree of corrosion on the properties of reinforcing steel bars », *Construction and Building Materials*, vol. 15, n° 8, p. 361-368, déc. 2001.
[36] T. Heitz, A. Le Maoult, B. Richard, C. Giry, et F. Ragueneau, « Dissipations in reinforced concrete components: Static and dynamic experimental identification strategy », *Engineering Structures*, vol. 163, p. 436-451, mai 2018.
[37] R. TC9-RC, « RILEM TC9-RC: RC6: Bond test for reinforcement steel. 2. Pull-out-test », *RILEM Technical recommendations for testing and use of construction materials. London: E& FN SPON*, p. 218-220, 1994.

[38] B. Richard, P. Martinelli, F. Voldoire, T. Chaudat, S. Abouri, et N. Bonfils, « SMART 2008: Overview, synthesis and lessons learned from the International Benchmark », *Engineering Structures*, vol. 106, p. 166-178, 2016.
[39] G. A. Papagiannopoulos et G. D. Hatzigeorgiou, « On the use of the half-power bandwidth method to estimate damping in building structures », *Soil Dynamics and Earthquake Engineering*, vol. 31, n° 7, p. 1075-1079, 2011.
[40] C. Lejouad, S. Capdevielle, B. Richard, et F. Ragueneau, « A numerical model to predict the effect of corrosion on the dynamic behavior of reinforced concrete beams », 12th Canadian Conference of Earthquake Engineering, 2019.